




Processivity of molecular motors under vectorial loads

Hamid Khataee ^{1,*}, Mohammed Mahamdeh ^{2,3,†} and Zoltan Neufeld ^{1,‡}

¹*School of Mathematics and Physics, The University of Queensland, St. Lucia, Brisbane, QLD 4072, Australia*

²*Harvard Medical School, Harvard University, Boston, Massachusetts 02115, USA*

³*Cardiovascular Research Center, Massachusetts General Hospital, Boston, Massachusetts 02129, USA*



(Received 27 April 2020; accepted 27 July 2020; published 18 August 2020)

Molecular motors are cellular machines that drive the spatial organization of the cells by transporting cargos along intracellular filaments. Although the mechanical properties of single molecular motors are relatively well characterized, it remains elusive how the geometry of a load imposed on a motor affects its processivity, i.e., the average distance that a motor moves per interaction with a filament. Here, we theoretically explore this question for a single-kinesin molecular motor by analyzing the load dependence of the stepping and detachment processes. We find that the processivity of the kinesin increases with lowering the load angle between the kinesin and the microtubule filament, due to the deceleration of the detachment rate. When the load angle is large, the processivity is predicted to enhance with accelerating the stepping rate through an optimal distribution of the load over the kinetic transition rates underlying a mechanical step of the motor. These results provide new insights into understanding of the design of potential synthetic biomolecular machines that can travel long distances with high velocities.

DOI: [10.1103/PhysRevE.102.022406](https://doi.org/10.1103/PhysRevE.102.022406)

I. INTRODUCTION

Kinesin, dynein, and myosin molecular motors exert localized forces on intracellular components by stepping directionally along intracellular filaments using the energy released from the hydrolysis of adenosine triphosphate (ATP) [1]. The motors have fundamental roles in several cellular processes [1]. For instance, they mediate the changes in and maintenance of the morphology of cells by directed transport of certain organelles [2] and sliding filaments along each other [3]. They also contribute to the movement of the cell body by transporting migration signals and controlling the cell polarity [4–6]. Accordingly, defects in the function of molecular motors cause various diseases, such as neurodegeneration and cancer [7,8]. Therefore a comprehensive understanding of the mechanical properties of molecular motors would provide new insights into the roles that motors play in health and disease.

A major factor that influences the function of a molecular motor in a three-dimensional (3D) cellular environment is the load applied on the motor due to, for example, blockages caused by other cellular components or thermal fluctuations of the cargo carried by a motor [9–12]. The vectorial character of the load $\mathbf{F} = (F_x, F_z)$ was established in experiments by Gittes *et al.* [13]. They measured the vertical load component F_z , where the horizontal component F_x was resisting (<0 , applied against the stepping direction); see Fig. 1. More recently, single-molecule optical trapping experiments [14–17] have studied the function of molecular motors under assisting loads

F_x (>0 , applied in the stepping direction) as well; see Fig. 1. They have shown that the motors exhibit similar responses to the applied load direction: (i) their velocity decreases with resisting loads but changes slightly when the load is assisting, and (ii) motors favor a faster detachment rate under assisting loads than resisting ones. The importance of this directionality comes from the need to understand the collective function of a complex of multiple motors under a vectorial load, which usually occurs within cells [18]. In such a complex, individual motors experience either resisting or assisting load due to intermolecular interactions. This reveals a need for understanding of the mechanics of single motors under vectorial applied loads.

The 3D vectorial character of applied loads was originally quantified by Fisher *et al.* [19,20]. They modeled single-kinesin load-velocity data [13,21] by quantifying the load dependence of the mechanical kinetics underlying a stepping process of the motor [19,20]. Recently, we also modeled the mechanics of force generation by kinesin motors by quantifying the detachment process of the motor as a function of an applied load vector \mathbf{F} [22]. These models of the stepping and detachment processes as functions of the geometry of an applied load suggest the kinesin motor as a system for modeling the processivity of molecular motors (i.e., the average distance that a motor moves per interaction with a filament [23–25]) under vectorial loads, which remains elusive.

Here we model the processivity of a single kinesin as a function of an applied load vector. We determine the processivity using kinetic transition rate models that illustrate the displacement of the motor body in the (x, z) domain during the stepping and detachment processes. The model describes how the distribution of the load components over the mechanochemical kinetics of the stepping and detachment processes determines the processivity.

*h.khataee@uq.edu.au

†mmahamdeh@mgh.harvard.edu

‡z.neufeld@uq.edu.au

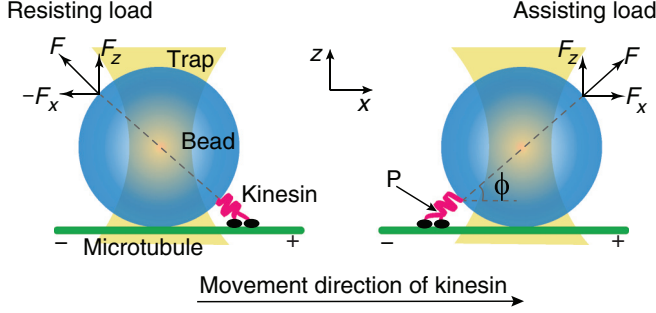


FIG. 1. A graphical illustration of a microtubule-kinesin-bead complex in a typical optical trap assay. Kinesin is attached to the bead (blue) with its tail (magenta) and moves, with its heads (black), along the microtubule (MT, green) toward the plus end under a resisting (left) or an assisting (right) load transmitted to the point P on the motor, which links its tail to its heads with an angle ϕ . Horizontal and vertical load components F_x and F_z are applied parallel and perpendicular to the MT axis, respectively.

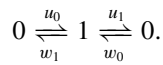
II. RESULTS AND DISCUSSION

The processivity of a single-kinesin motor with a mean run length

$$l = \frac{v}{k_{\text{off}}}, \quad (1)$$

is maximized if the velocity v of the motor is high and the detachment rate k_{off} of the motor from a microtubule (MT) is low. This means that the relationship between the processivity and the vectorial character of the applied load depends on the role of the load in two processes: (i) stepping, which determines the velocity v , and (ii) detachment, which determines the run time ($1/k_{\text{off}}$, average time to detachment). Therefore to model the load-processivity relationship, we analyze the load-velocity and load-detachment rate relationships. We use Andreasson *et al.* experimental data [14], as it provides measurements of velocity, detachment rate, and run length under resisting and assisting loads.

First, the effect of the vectorial character of the load on the velocity is described using a two-state transition rate model developed for an individual stepping cycle of the motor [19,26]. This transition rate model describes a forward step of length $d = 8.2$ nm as passing through a sequence of two mechanochemical states 0 (ATP free) and 1 (ATP processing) [19]:



One complete forward transition corresponds to a forward step of the motor and the hydrolysis of an ATP molecule to its products, adenosine diphosphate (ADP) and inorganic phosphate (P_i). Likewise, one complete reverse transition includes a backward step and the synthesis of ATP from ADP and P_i [20,27]. The forward and backward transition rates are given by [19,20]

$$u_j(\mathbf{F}) = u_j^0 e^{\theta_j^+ \cdot \mathbf{F}d/k_B T}, \quad (2)$$

$$w_j(\mathbf{F}) = w_j^0 e^{-\theta_j^- \cdot \mathbf{F}d/k_B T}, \quad (3)$$

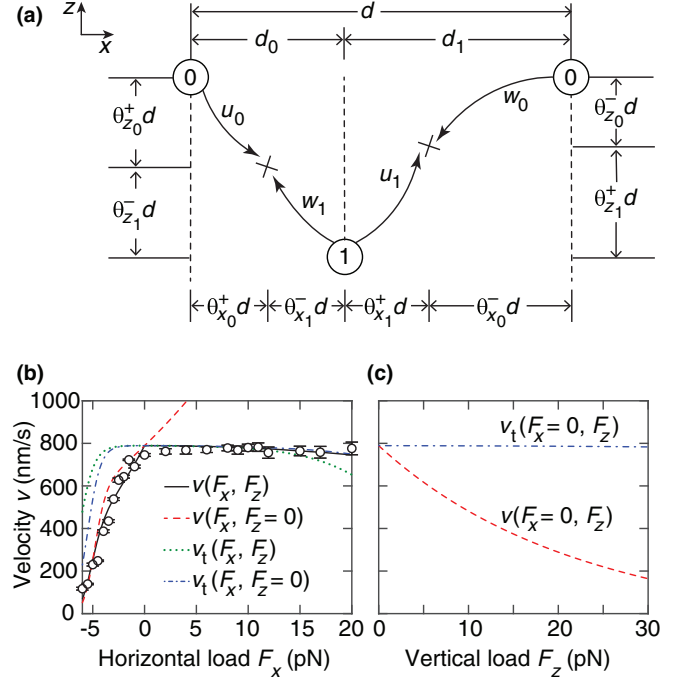


FIG. 2. Velocity of a single kinesin. (a) Schematic of the two-state stepping transition rate model from [19]. States 0 and 1: ATP-free and ATP-processing states, respectively. Crosses: Transition states. (b) Velocity v vs the horizontal load component F_x . Open circles: Experimental data (mean \pm SE) at saturating 2 mM ATP [14]. Solid curve: v where the motor is subject to both F_x and F_z , calculated using Eq. (4). Dashed curve: v when the applied load \mathbf{F} is horizontal. Dotted curve: v_t denotes the velocity v when $\theta_0^+ \rightarrow 0$ and $\theta_1^+ \rightarrow 0$. Dashed-dotted curve: v_t when \mathbf{F} is horizontal. (c) v vs the vertical load component F_z (dashed curve). Dashed-dotted curve: v_t .

where u_j^0 and w_j^0 are the unloaded rates, $\theta_j^+ = (\theta_{x_j}^+, \theta_{z_j}^+)$ and $\theta_j^- = (\theta_{x_j}^-, \theta_{z_j}^-)$ are the dimensionless load sharing factors (for $j = 0, 1$), and $k_B T$ is the thermal energy. The velocity is then given by [20]

$$v(\mathbf{F}) = \frac{d(u_0 u_1 - w_0 w_1)}{u_0 + u_1 + w_0 + w_1}. \quad (4)$$

The parameter values of Eq. (4) have been estimated by fitting to the experimental data of Block and colleagues [21]. The unloaded rates take $u_0^0 = k_0[\text{ATP}]$, where $k_0 = 1.35 \mu\text{M}^{-1} \text{s}^{-1}$, $w_1^0 = 5 \text{s}^{-1}$, $u_1^0 = 100 \text{s}^{-1}$, and $w_0^0 = k'_0[\text{ATP}]/(1 + [\text{ATP}]/c_0)^{1/2}$, where $k'_0 = 2.04 \times 10^{-3} \mu\text{M}^{-1} \text{s}^{-1}$ and $c_0 = 20 \mu\text{M}$ [19]. The load distribution vectors in the (x, z) plane are [19]

$$\begin{aligned} \theta_0^+ d &= (0.98, -0.38) \text{ nm}, \\ \theta_1^+ d &= (-0.83, -0.27) \text{ nm}, \\ \theta_1^- d &= (0.26, -0.23) \text{ nm}, \\ \theta_0^- d &= (7.79, 0.88) \text{ nm}, \end{aligned} \quad (5)$$

where the load distribution factors $(\theta_{x_0}^+ + \theta_{x_1}^- + \theta_{x_1}^+ + \theta_{x_0}^-) = 1$ and $(\theta_{z_0}^+ + \theta_{z_1}^- + \theta_{z_1}^+ + \theta_{z_0}^-) = 0$ demonstrate the motion of the attachment point P in the (x, z) domain; see Fig. 2(a). They also indicate how the load is shared between the forward

and backward rates according to the location of the kinetic transition states (i.e., the saddle points in the free-energy landscape) between states 0 and 1 [19,27]. The transition states before and after ATP binding are located at $\theta_{x_0}^+ d$ and $d_0 + \theta_{x_1}^+ d$ along the MT axis, respectively [19]. Using this two-state stepping transition rate model, it was found that the velocity generally decreases with increasing F_z [19,26] rather than increases, as argued in the MT buckling experiments [13]. It was reasoned that in the MT buckling experiments the kinesin moves away from a curved (stressed) region of the MT and that curvature of the MT might affect the motility of the kinesin [26].

The location of a transition state was also found to affect the velocity: the kinesin moves faster when a transition state is close to the initial state [27–30]. The applied load increases the height of the kinetic barriers, making it more difficult to transition between states and thus slowing down the velocity of the motor [28]. Therefore, if the distance to a transition state is zero, the load does not increase the height of the kinetic barrier along a mechanical step of the motor.

We analyze the effects of both the load angle ϕ and the locations of the transition states on velocity. Experiments in [14] were performed with an optical force clamp, where the load applied by the trap is a function of the displacement of the motor in the x direction [31]. Therefore we model the load-dependent velocity data [14] using Eq. (4) and the ansatz $F_z = F_x \tan \phi$; see Fig. 2(b), solid curve. For a 440-nm-diameter bead and a 35-nm-long kinesin used in the experiments [14], we use our earlier estimated kinesin-MT

angle $\phi \sim 60^\circ$, where for simplicity it is assumed that the bead is adjacent to the surface of the MT [22]. Thermal fluctuations of the bead [32,33] will have negligible effect on the vectorial load-run length calculations, as the perpendicular fluctuations (~ 5 nm [19,32]) correspond to $\sim 1^\circ$ change in ϕ . This simplification, however, enables us to use the fit parameters for the vectorial load-velocity and load-detachment rate relationships as estimated in [19,22]. It is also assumed that the stiffness of the kinesin will not significantly affect ϕ . Experiments have shown that the stiffness of a single kinesin changes from ~ 0.05 to ~ 0.2 pN/nm when the applied load changes from -1 to -6 pN [34]. This would lead to $\sim 3^\circ$ change in ϕ .

We find that for horizontal loads, the velocity increases, especially when the load is assisting; see Fig. 2(b), dashed curve. But for vertical loads, velocity decreases; Fig. 2(c), dashed curve. We also find that the velocity increases under all load geometries when the distance to the transition states approaches zero, i.e., $\theta_0^+ \rightarrow 0$ and $\theta_1^+ \rightarrow 0$; see Fig. 2(b), dotted and dashed-dotted curves and Fig. 2(c) dashed-dotted curve. Together, these results suggest that velocity increases under various applied load geometries with lowering the distance to transition states. In this regime, an enhancement in velocity is predicted under resisting loads. For vertical loads, the velocity remains almost load independent.

To model the effect of the vectorial character of the load on the detachment process, we follow our model [22] that describes the detachment of a kinesin from a MT as a two-step process which passes through three states:

strongly bound state $\xrightarrow{k_1}$ weakly bound state $\xrightarrow{k_2}$ detached state.

k_1 and k_2 are the fast and slow detachment rates, respectively, that depend on the load \mathbf{F} and displacement $\delta_j = (\delta_{x_j}, \delta_{z_j})$ vectors according to

$$k_j = k_j^0 e^{\mathbf{F} \cdot \delta_j / k_B T}, \quad (6)$$

where k_j^0 (for $j = 1, 2$) are the unloaded rates. The effective detachment rate is then given by [22]

$$k_{\text{off}}(\mathbf{F}) = \frac{k_1 k_2}{k_1 + k_2}. \quad (7)$$

By fitting Eq. (7) to the load-detachment rate data [14], the two-step detachment model described the data by a continuous curve, where $k_1^0 = 0.91 \pm 0.38$ s $^{-1}$, $\delta_{x_1} = 2.90 \pm 1.24$ nm, $\delta_{z_1} = 2.25 \pm 0.75$ nm, $k_2^0 = 7.62 \pm 0.74$ s $^{-1}$, and $\delta_{z_2} = 0.18 \pm 0.01$ nm (mean \pm SE) [22]. This two-step model explained the effects of the load geometry on the detachment process [22]: (i) the detachment rate decreases with horizontal loads (i.e., catch-bond behavior) when it is resisting and increases for assisting loads [see Fig. 3(a), dashed curve]; and (ii) detachment rate increases with vertical loads [i.e., slip-bond behavior, see Fig. 3(b)]. Using these catch and slip bonding mechanisms, we explained different behaviors of kinesin motors reported from different laboratories [22]. It explained that the stall force of multiple kinesins can be similar to that of a single kinesin when the vertical load component is high,

as observed in [34,35], due to slip-bond behavior. However, multiple kinesins can produce forces much larger than the single-motor force when the vertical load component is small, e.g., in gliding assays [36,37] and bead assays [38–40], due to catch-bond behavior. This later prediction has been recently confirmed in a three-bead assay where lower detachment rates were observed for a single kinesin with a low kinesin-MT angle [41].

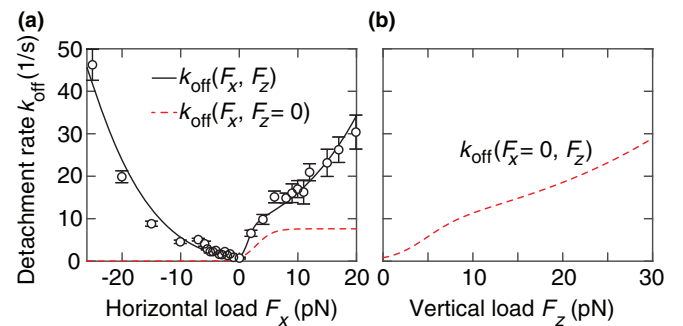


FIG. 3. Detachment rate of a single kinesin. (a) Detachment rate k_{off} vs F_x . Open circles: Experimental data (mean \pm SE) from [14]. Solid curve: k_{off} calculated using Eq. (7), where the motor is subject to both F_x and F_z . Dashed curve: k_{off} when \mathbf{F} is parallel to the MT axis. (B) k_{off} when \mathbf{F} is perpendicular to the MT axis.

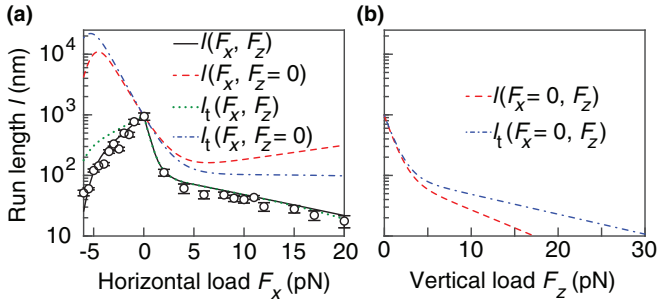


FIG. 4. Run length of a single kinesin. (a) Run length l vs F_x . Open circles: Experimental data (mean \pm SE) from [14]. Solid curve: l , where the motor is subject to both F_x and F_z , derived using Eq. (1). Dashed curve: l when F is horizontal. Dotted curve: l_t denotes the run length when $\theta_0^+ \rightarrow 0$ and $\theta_1^+ \rightarrow 0$. Dashed-dotted curve: l_t when F is horizontal. (b) l vs F_z (dashed curve). Dashed-dotted curve: l_t .

We now model the processivity of the kinesin by analyzing the dependencies of the stepping and detachment processes to the load components. We find that the processivity increases over all resisting and assisting loads with lowering the kinesin-MT angle; see Fig. 4(a). This is explained by the acceleration of the velocity and the catch-bond behavior of the motor; see Figs. 2(b) and 3(a). In addition, decreasing the distance to the stepping kinetic transition states enhances the run length over resisting loads; see Fig. 4(a). This is due to the increase in the velocity of the motor. For vertical loads, we find a fast decrease in the processivity. This can be reasoned in that the velocity of the motor is limited by a high detachment rate due to slip-bond behavior. For example, under a vertical load of 20 pN, while the kinesin can step with a moderate velocity [Fig. 2(b), dashed curve], the run length < 10 nm [Fig. 4(b), dashed red], resembling a fast detachment [Fig. 3(b), dashed curve] after attaching to the MT. We also find that lowering the distance to the stepping kinetic transition states is predicted to benefit the run length; see Fig. 4(b). Small distances to transition states results in an almost steady velocity, while the motor exhibits slip-bond behavior; see Figs. 2(c) and 3(b).

We conclude that a motor with longer body length (for a fixed size of cargo), where distances to stepping transition states are small, can travel long distances with high velocities; see Figs. 2(b) and 4(a), dashed-dotted blue curve. Such motors exhibit catch-bond behavior with faster stepping rates. On the other hand, the run length of a motor is minimized when the motor body is short and the distances to the stepping transition states are large. Such motors would step with slow rates and are more likely to exhibit slip-bond behavior. An *in vivo* implication of this prediction is that motors with different mechanical properties can exhibit different processivities in carrying cargos with different sizes.

In this study we modeled the processivity of a single kinesin motor under vectorial applied load geometries by taking into account the load-dependent dynamics of the stepping and detachment processes. We found that the processivity of the kinesin increases with lowering the vertical component of the load. This is explained by the catch-bond behavior that allows the kinesin to stay attached to the MT under high loads F_x . This behavior has been observed in recent experiments where the effects of horizontal and vertical loads on the attachment duration of a single kinesin were investigated using a three-bead assay [41]. When the kinesin was subject to horizontal loads, a threefold increase in the attachment duration was observed. The run length of a single kinesin molecule under loads with different vertical components can be measured by running similar experiments in a force clamp mode, analogous to the experiments performed on myosin motors [15,42,43]. Our model also predicted that when the vertical load component is large, processivity can be enhanced with accelerating the stepping rate through an optimal load distribution over the stepping transition rates.

Future works may consider the effects of the backward stepping (velocity) of the motor on its processivity upon the availability of the velocity and detachment rate data over high resisting and assisting loads. Backward steps of the kinesin, on average, are driven by ATP hydrolysis at loads above the stalling conditions [10,44–47], although ATP synthesis can result in backward stepping [19,20].

The dependence of the vectorial load-processivity relationship on the ATP concentration can also be analyzed. Although the run length at different ATP concentrations has been measured under a moderate assisting load (4 pN) [48], modeling such a relationship would require a comprehensive load- and ATP-dependent detachment rate data. Such data can further be incorporated into the earlier computational models (e.g., [47,49]) to analyze the affinity of the motor for MTs in different kinetic states under a vectorial load.

The present model can be helpful in quantifying the effects of the vectorial character of the applied load on the mechanics of dynein and myosin motors, since the load-velocity and load-detachment rate behaviors of kinesins, dyneins, and myosins are similar [14–17]. This can help to understand the mechanics of the collective function of different molecular motors, owing to the force-dependent interactions of the motors. It will further provide new insights into exploring the design of synthetic molecular machines powered by molecular motors [50] that can operate with high efficiency in a 3D environment.

ACKNOWLEDGMENT

We are grateful to Jonathon Howard for comments and suggestions.

- [1] J. Howard, *Mechanics of Motor Proteins and the Cytoskeleton* (Sinauer, Sunderland, MA, 2001).
 [2] V. I. Rodionov, Microtubule-dependent control of cell shape and pseudopodial activity is inhibited by the antibody to kinesin motor domain, *J. Cell Biol.* **123**, 1811 (1993).

- [3] A. L. Jolly, H. Kim, D. Srinivasan, M. Lakonishok, A. G. Larson, and V. I. Gelfand, Kinesin-1 heavy chain mediates microtubule sliding to drive changes in cell shape, *Proc. Natl. Acad. Sci. USA* **107**, 12151 (2010).

- [4] J.-B. Manneville, M. Jehanno, and S. Etienne-Manneville, Dlg1 binds GKAP to control dynein association with microtubules, centrosome positioning, and cell polarity, *J. Cell Biol.* **191**, 585 (2010).
- [5] A. Bachmann and A. Straube, Kinesins in cell migration, *Biochem. Soc. T.* **43**, 79 (2015).
- [6] R. B. Vallee, G. E. Seale, and J.-W. Tsai, Emerging roles for myosin II and cytoplasmic dynein in migrating neurons and growth cones, *Trends Cell Biol.* **19**, 347 (2009).
- [7] A. J. Lucanus and G. W. Yip, Kinesin superfamily: Roles in breast cancer, patient prognosis and therapeutics, *Oncogene* **37**, 833 (2018).
- [8] S. T. Brady and G. A. Morfini, Regulation of motor proteins, axonal transport deficits and adult-onset neurodegenerative diseases, *Neurobiol. Dis.* **105**, 273 (2017).
- [9] M. J. Schnitzer, K. Visscher, and S. M. Block, Force production by single kinesin motors, *Nat. Cell Biol.* **2**, 718 (2000).
- [10] N. J. Carter and R. A. Cross, Mechanics of the kinesin step, *Nature (London)* **435**, 308 (2005).
- [11] A. Gennerich, A. P. Carter, S. L. Reck-Peterson, and R. D. Vale, Force-induced bidirectional stepping of cytoplasmic dynein, *Cell* **131**, 952 (2007).
- [12] A. D. Mehta, R. S. Rock, M. Rief, J. A. Spudich, M. S. Mooseker, and R. E. Cheney, Myosin-V is a processive actin-based motor, *Nature (London)* **400**, 590 (1999).
- [13] F. Gittes, E. Meyhöfer, S. Baek, and J. Howard, Directional loading of the kinesin motor molecule as it buckles a microtubule, *Biophys. J.* **70**, 418 (1996).
- [14] J. O. Andreasson, B. Milic, G.-Y. Chen, N. R. Guydosh, W. O. Hancock, and S. M. Block, Examining kinesin processivity within a general gating framework, *eLife* **4**, e07403 (2015).
- [15] L. Gardini, S. M. Heissler, C. Arbore, Y. Yang, J. R. Sellers, F. S. Pavone, and M. Capitanio, Dissecting myosin-5B mechanosensitivity and calcium regulation at the single molecule level, *Nat. Commun.* **9**, 2844 (2018).
- [16] S. Can, S. Lacey, M. Gur, A. P. Carter, and A. Yildiz, Directionality of dynein is controlled by the angle and length of its stalk, *Nature (London)* **566**, 407 (2019).
- [17] Y. Ezber, V. Belyy, S. Can, and A. Yildiz, Dynein harnesses active fluctuations of microtubules for faster movement, *Nat. Phys.* **16**, 312 (2020).
- [18] E. L. Holzbaur and Y. E. Goldman, Coordination of molecular motors: From in vitro assays to intracellular dynamics, *Curr. Opin. Cell Biol.* **22**, 4 (2010).
- [19] M. E. Fisher and Y. C. Kim, Kinesin crouches to sprint but resists pushing, *Proc. Natl. Acad. Sci. USA* **102**, 16209 (2005).
- [20] M. E. Fisher and A. B. Kolomeisky, Simple mechanochemistry describes the dynamics of kinesin molecules, *Proc. Natl. Acad. Sci. USA* **98**, 7748 (2001).
- [21] S. M. Block, C. L. Asbury, J. W. Shaevitz, and M. J. Lang, Probing the kinesin reaction cycle with a 2D optical force clamp, *Proc. Natl. Acad. Sci. USA* **100**, 2351 (2003).
- [22] H. Khataee and J. Howard, Force Generated by Two Kinesin Motors Depends on the Load Direction and Intermolecular Coupling, *Phys. Rev. Lett.* **122**, 188101 (2019).
- [23] J. Howard, A. J. Hudspeth, and R. D. Vale, Movement of microtubules by single kinesin molecules, *Nature (London)* **342**, 154 (1989).
- [24] R. D. Vale, T. Funatsu, D. W. Pierce, L. Romberg, Y. Harada, and T. Yanagida, Direct observation of single kinesin molecules moving along microtubules, *Nature (London)* **380**, 451 (1996).
- [25] S. M. Block, L. S. B. Goldstein, and B. J. Schnapp, Bead movement by single kinesin molecules studied with optical tweezers, *Nature (London)* **348**, 348 (1990).
- [26] Y. C. Kim and M. E. Fisher, Vectorial loading of processive motor proteins: Implementing a landscape picture, *J. Phys.: Condens. Matter* **17**, S3821 (2005).
- [27] J. A. Wagoner and K. A. Dill, Molecular motors: Power strokes outperform Brownian ratchets, *J. Phys. Chem. B* **120**, 6327 (2016).
- [28] J. Howard, Motor proteins as nanomachines: The roles of thermal fluctuations in generating force and motion, in *Biological Physics* (Springer, Basel, 2011), pp. 47–59.
- [29] J. A. Wagoner and K. A. Dill, Mechanisms for achieving high speed and efficiency in biomolecular machines, *Proc. Natl. Acad. Sci. USA* **116**, 5902 (2019).
- [30] T. Schmiedl and U. Seifert, Efficiency of molecular motors at maximum power, *Europhys. Lett.* **83**, 30005 (2008).
- [31] K. Visscher, C. Block, S. M. Keller, F. Berger, S. Liepelt, and R. Lipowsky, Versatile optical traps with feedback control, *Methods Enzymol.* **298**, 460 (1998).
- [32] K. Svoboda and S. M. Block, Force and velocity measured for single kinesin molecules, *Cell* **77**, 773 (1994).
- [33] E. Schäffer, S. F. Nørrelykke, and J. Howard, Surface forces and drag coefficients of microspheres near a plane surface measured with optical tweezers, *Langmuir* **23**, 3654 (2007).
- [34] D. K. Jamison, J. W. Driver, A. R. Rogers, P. E. Constantinou, and M. R. Diehl, Two kinesins transport cargo primarily via the action of one motor: Implications for intracellular transport, *Biophys. J.* **99**, 2967 (2010).
- [35] K. Furuta, A. Furuta, Y. Y. Toyoshima, M. Amino, K. Oiwa, and H. Kojima, Measuring collective transport by defined numbers of processive and nonprocessive kinesin motors, *Proc. Natl. Acad. Sci. USA* **110**, 501 (2013).
- [36] V. Bormuth, A. Jannasch, M. Ander, C. M. van Kats, A. van Blaaderen, J. Howard, and E. Schäffer, Optical trapping of coated microspheres, *Opt. Express* **16**, 13831 (2008).
- [37] A. Hunt, F. Gittes, and J. Howard, The force exerted by a single kinesin molecule against a viscous load, *Biophys. J.* **67**, 766 (1994).
- [38] G. T. Shubeita, S. L. Tran, J. Xu, M. Vershinin, S. Cermelli, S. L. Cotton, M. A. Welte, and S. P. Gross, Consequences of motor copy number on the intracellular transport of kinesin-1-driven lipid droplets, *Cell* **135**, 1098 (2008).
- [39] M. Vershinin, B. C. Carter, D. S. Razafsky, S. J. King, and S. P. Gross, Multiple-motor based transport and its regulation by tau, *Proc. Natl. Acad. Sci. USA* **104**, 87 (2007).
- [40] M. Bovyn, S. Gross, and J. Allard, Molecular motor organization and mobility on cargos can overcome a tradeoff between fast binding and run length, *Biophys. J.* **118**, 607a (2020).
- [41] S. Pyrpapopoulos, H. Shuman, and E. M. Ostap, Modulation of kinesin's load-bearing capacity by force geometry and the microtubule track, *Biophys. J.* **118**, 243 (2020).
- [42] M. Capitanio, M. Canepari, M. Maffei, D. Beneventi, C. Monico, F. Vanzi, R. Bottinelli, and F. S. Pavone, Ultrafast force-clamp spectroscopy of single molecules reveals load dependence of myosin working stroke, *Nat. Methods* **9**, 1013 (2012).

- [43] R. S. Rock, S. E. Rice, A. L. Wells, T. J. Purcell, J. A. Spudich, and H. L. Sweeney, Myosin VI is a processive motor with a large step size, *Proc. Natl. Acad. Sci. USA* **98**, 13655 (2001).
- [44] M. Nishiyama, H. Higuchi, and T. Yanagida, Chemomechanical coupling of the forward and backward steps of single kinesin molecules, *Nat. Cell Biol.* **4**, 790 (2002).
- [45] H. Khataee and A. W.-C. Liew, A stochastic automaton model for simulating kinesin processivity, *Bioinformatics* **31**, 390 (2015).
- [46] S. Liepelt and R. Lipowsky, Kinesin's Network of Chemomechanical Motor Cycles, *Phys. Rev. Lett.* **98**, 258102 (2007).
- [47] H. Khataee, S. Naseri, Y. Zhong, and A. W.-C. Liew, Unbinding of kinesin from microtubule in the strongly bound state enhances under assisting forces, *Mol. Inf.* **37**, 1700092 (2018).
- [48] B. Milic, J. O. L. Andreasson, W. O. Hancock, and S. M. Block, Kinesin processivity is gated by phosphate release, *Proc. Natl. Acad. Sci. USA* **111**, 14136 (2014).
- [49] C. Keller, F. Berger, S. Liepelt, and R. Lipowsky, Network complexity and parametric simplicity for cargo transport by two molecular motors, *J. Stat. Phys.* **150**, 205 (2013).
- [50] H. Hess, Toward devices powered by biomolecular motors, *Science* **312**, 860 (2006).